Performance of a real-time photon counting optical receiver in the presence of emulated channel fading

Jennifer N. Downey*, Yousef K. Chahine, Sarah A. Tedder, Evan J. Katz, Michael A. Marsden, John S. Clapham
NASA Glenn Research Center, 21000 Brookpark Road, Cleveland, Ohio 44135

ABSTRACT

Free-space optical communication links with terrestrial ground stations experience fading due to atmospheric scintillation and beam pointing. Fiber-coupled receiver systems experience additional fading at the interface between the fiber and free-space optics of the telescope. The National Aeronautics and Space Administration (NASA) Glenn Research Center (GRC) has characterized a real-time photon-counting optical ground receiver system with an atmospheric fade emulation system. The receiver system is comprised of a fiber interconnect, an array of superconducting nanowire single photon detectors (SNSPDs), and a field programmable gate array (FPGA) based receive modem. Two fiber interconnect/detector architectures have been studied. One architecture uses a 70-mode photonic lantern coupled to seven single pixel SNSPDs. The other architecture uses a 10-mode few-mode fiber (FMF) coupled to a 15-pixel SNSPD array. The receiver system complies with the Consultative Committee for Space Data Systems (CCSDS) Optical Communications High Photon Efficiency Coding and Synchronization Standard, which uses serially concatenated convolutionally coded pulse-position modulation (SCPPM). The CCSDS standard is designed for use in low photon flux missions, including the Orion Artemis-II Optical (O2O) communications demonstration. The standard utilizes a convolutional symbol interleaver which can be resized to mitigate different fades. The fade emulation system employed in this work emulates scintillation-induced, pointing-induced, and coupling-induced fading. This paper gives an overview of the real-time optical receiver system and the fade emulation system. It presents tests results which show the impact of fading on the performance on the receiver. The test results show that in the presence of channel fading, the 70-mode photonic lantern outperforms the 10-mode FMF under higher ($D/r_0 = 9$) turbulence conditions due to high fiber-coupling-induced fading and fiber coupling loss on the 10-mode FMF. When operating in lower turbulence ($D/r_0 = 4$), the 10-mode FMF outperforms the 70-mode photonic lantern. The paper also shows a larger convolutional interleaver improves the system performance as long as the receiver does not lose acquisition.

Keywords: Optical communications, pulse-position modulation, convolutional interleaving, emulation, fading, fade statistics

1. INTRODUCTION

The NASA Glenn Research Center (GRC) is prototyping a photon counting receiver system compliant with the Consultative Committee for Space Data Systems (CCSDS) Optical Communications High Photon Efficiency (HPE) Standard.[1] The receiver system is modular, scalable, and comprised of mostly commercial off the shelf (COTS) components. The receiver system consists of a fiber interconnect, superconducting nanowire single photon counting detectors (SNSPDs), and a field programmable gate array (FPGA) based receive modem. The performance of two receiver architectures was studied. The first architecture utilizes a 70-mode photonic lantern with 7 legs connected to 7 single-pixel detectors. The second architecture is comprised of a 10-mode few-mode fiber (FMF) coupled to a monolithic 16-channel SNSPD array. Both architectures utilize an FPGA-based platform for timing recovery, deinterleaving, decoding and deframing.

*Send correspondence to jennifer.n.downey@nasa.gov

The CCSDS HPE standard uses serially concatenated convolutionally coded pulse-position modulation (SCPPM), with code rates of 1/3, 1/2, or 2/3 and pulse-position modulation (PPM) orders of 4, 8, 16, 32, 64, 128, and 256. PPM pulse widths range from 512 ns to 125 ps so that the maximum data rate supported is ~2 Gbps. The CCSDS HPE standard utilizes a convolutional symbol interleaver to mitigate channel fading. The interleaver has N rows of length iB, where i is the row number and B defines row length. The convolutional interleaver size is designed to mitigate channel fading. There are several main sources of channel fading including scintillation and pointing-induced fading[2][2]. Another source of fading is unique to fiber-coupled receiver systems: fiber-coupling-induced fading. This fading is caused by energy being scattered into higher order spatial modes by atmospheric effects. The fiber-coupling-induced fading is impacted by the size of the fiber core into which light is coupled.

This paper compares the emulated nighttime performance of the receiver architectures at a ground station site in Greenbelt, Maryland. An overview of the receiver system is given in section 2. A description of the hardware fade emulation system is given in 3. The expected atmospheric conditions at the ground station were modeled as they apply to both architectures. A description of the fade model used to generate fades is given in section 4. The experimental test setup is described in section 5. Test results for both receiver architectures are given in section 6.

2. RECEIVER SYSTEM OVERVIEW

The receiver system consists of a fiber interconnect, SNSPDs, and a FPGA-based receive modem. Light from the backend optics of the telescope is coupled into the receiver system at the fiber interconnect. The receiver system has been previously described[3][3], but a brief overview is given here.

Two fiber interconnect/detector architectures have been prototyped and tested in the laboratory.[4][4] The first architecture consists of a photonic lantern with a 55 µm core diameter input supporting 70 modes and seven few mode fiber (FMF) output legs. Each FMF is graded index, has a 25 µm core, and supports the first 10 linearly polarized (LP) modes per polarization counting parity. Each output leg is butt-coupled to a FMF with a graded index 20 µm diameter supporting 6 LP modes. Each of these fibers are then butt-coupled to a single-pixel SNSPD. The single-pixel SNSPD output pulses have a rise time of about 850 ps and a 1/*e* reset time on the order of 15 ns.

The second architecture consists of a 25 µm single FMF (10 LP modes) coupled to a graded index 20 µm diameter FMF supporting 6 LP modes. This fiber is butt-coupled to the multi-channel SNSPD array. The array output pulse rise times are on average 500 ps, with $1/$ reset times in the 5 – 8 ns range. The array was designed to have 16 channels, but the left-most channel was not functional, so 15 channels were used in this work.

The FPGA-based receive modem[5] [5]is implemented on two COTS FPGA cards housed in a Micro Telecommunications Architecture (MicroTCA) chassis. One FPGA card is used for detector channel alignment and combining, symbol timing recovery, codeword alignment, and symbol deinterleavering. Previously, detector channel time alignment was performed externally to the FPGA using phase shifters. This function has been moved into the FPGA, which can compensate for maximum path differences of 1 ns. Symbol deinterleaving starts when the timing recovery loop has acquired the beginning of the symbols and the codeword synchronization marker has been located to track the beginning of each codeword. The deinterleaver works by reading a symbol from a memory location, and then writing a symbol to a memory location. Initially, the symbols are read from locations that have not yet been filled with new symbols. Therefore, the initial contents of memory must be cleared, which takes $NB(N-1)$ symbol reads. The second FPGA card is used for iterative decoding, derandomization and deslicing.

3. FADE EMULATION SYSTEM

The fade emulation system, shown in Figure 1, consists of three main components: a computer running a channel fade model in real time for generating fade vectors, a digital-to-analog converter (DAC), and an acousto-optic modulator (AOM). The discrete-time fading signal is synthesized in real-time and converted to a digital voltage signal $V[m]$ based on a transfer function constructed from the response of the acousto-optic modulator.[6][6] This signal is sent to the 16-bit DAC at a sample rate of 10 ksamples/s. The output of the DAC drives the AOM which is used to modulate the optical signal from the test transmitter. The AOM is a polarization-maintaining fiber-coupled commercial-off-the-shelf device

with an advertised maximum 55 MHz response, 45 dB of range, with optical operation within the c-band (1550 nm). Characterization of the acousto-optic modulator was previously reported.[7][7]

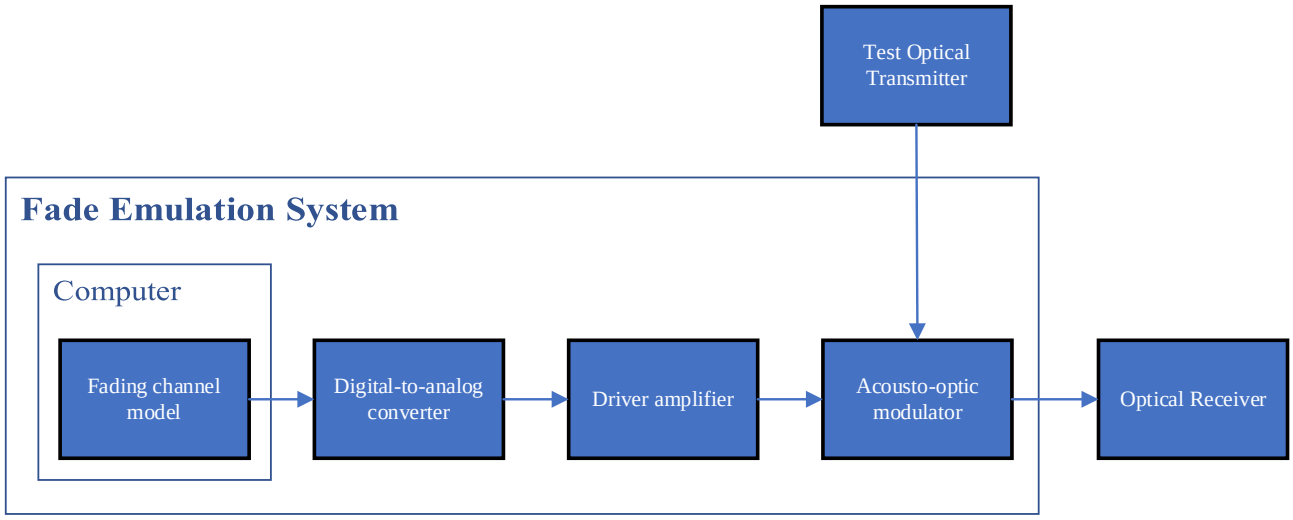

Figure 1. The fade emulation system hardware consists of a computer, DAC, driver amplifier, and AOM.

4. FADING CHANNEL MODEL

Three sources of channel fade are modeled:

1. scintillation-induced fade (SIF) from aperture-averaged atmospheric scintillation (η_s),
2. pointing-induced fade (PIF) from transmitter pointing error (η_p), and
3. fiber coupling-induced fade (CIF) from uncompensated turbulent optical field distortions (η_c).

Each source of fade is treated as an independent stochastic process $\eta_s(t), \eta_p(t)$, and $\eta_c(t)$, respectively. Each process is independently generated as a discrete-time signal sampled at 10 ksamples/s and combined to form the overall channel fade vector

$$\eta[m] = \eta_s[m]\eta_p[m]\eta_c[m].$$

Each process is synthesized based on a model for the probability density function (pdf), discussed in the following subsections, and power spectral density (psd), defined as

$$\Phi(f) = \frac{1}{1 + (f/f_c)^{\alpha}}$$

which is parameterized by a cutoff frequency f_c and power-law roll-off with logarithmic slope α. The remainder of this section summarizes the assumptions/parameterization of the channel. Details of this parametric fade model have been previously documented.[7]

4.1 Scintillation-induced fade (SIF): Log-normal distribution

In this work, we model atmospheric scintillation assuming a space-to-ground downlink with a 70 cm diameter receiving telescope. For a 70 cm aperture, scintillation effects are strongly suppressed due to aperture-averaging. A weak scintillation model is thus employed assuming log-normal received power fluctuations with power scintillation index $\sigma_I^2 = 0.025$ based on typical atmospheric turbulence profiles over a low elevation path. This is also consistent with measurements of weak-to-strong scintillation for a LEO downlink with a 40 cm receiving aperture reported by Eppel.[8] A power law roll-off of 40 dB/decade ($\alpha = 4$) is chosen to model the psd of the aperture-averaged fluctuations in the large-aperture regime.[7][7]

Scintillation fade vectors for the following tests are generated using a cutoff frequency $f_c = 220$ Hz corresponding to a half-width at half maximum (HWHM) atmospheric correlation time $\tau_C = 1$ ms.

4.2 Pointing-induced fade (PIF): Beta distribution

Due to the high directionality of an optical laser communications beam, pointing error due to spacecraft platform jitter can lead to fluctuations in the beam intensity at the ground receiver which depend on the ratio of the $1/e^2$ divergence half-angle w_0 to the root mean square (rms) angular pointing error σ_j. Assuming the transmitter produces a Gaussian beam such that the angular pointing jitter is Gaussian in two orthogonal axes (without pointing bias), the power distribution at a point receiver normalized to the on-axis beam irradiance takes the form of a beta distribution[2]

$$p(x;\beta) = \beta x^{\beta-1}$$

where $\beta = w_0^2/4\sigma_j^2$. Accounting for jitter (without pointing bias), the average received power is reduced from the on-axis irradiance by the factor $\beta/(\beta+1)$. In this work, we model a pointing, acquisition, and tracking (PAT) system targeting a jitter ratio with $\beta = 16$ for the communications beam, corresponding to a PAT budget allowing an average loss of 0.26 dB associated to pointing jitter. For a beam with far-field divergence, $w_0 = 10.5$ μrad. This corresponds to rms jitter of $\sigma_j = 2.6$ μrad. The temporal statistics of the pointing fluctuations are modeled assuming two independent single-axis angular pointing PSDs with 3 dB cutoff frequency of 10 Hz and roll-off slope of 20 dB/decade ($\alpha = 2$).

4.3 Coupling-induced fade (CIF): Weibull distribution

For a fiber-coupled receiver without adaptive optics, the average amount of light that can be accepted into the fiber depends on the ratio between the number of modes M guided by the fiber and the ratio D/r_0 relating the telescope diameter to the atmospheric coherence diameter r_0. One generally requires $M > (D/r_0)^2$ to collect all the light from the receiving aperture into the fiber.[9,10] For mode-limited systems which cannot meet this requirement, i.e. $M < (D/r_0)^2$, the amount of light from the telescope which is collected by the fiber at a given instant fluctuates depending primarily on the atmospheric turbulence-induced distortion of the phase of the optical field across the telescope aperture.[7]

The cutoff frequency for coupling-induced fade can be estimated from the Greenwood frequency f_G together with D/r_0. To this end, we define an effective phase velocity

$$V_\phi \equiv \frac{\left(\int C_n^2(s) v(s)^{5/3} ds\right)^{3/5}}{\left(\int C_n^2(s) ds\right)^{3/5}} = 2.34\, r_0 f_G$$

where $C_n^2(s)$ and $v(s)$ are the refractive index structure constant and transverse wind speed at position s along the propagation path, respectively. Following Chahine, Katz, Vyhnalek, and Tedder[7] we estimate the cutoff frequency f_c in terms of the characteristic frequency $f_\phi = V_\phi/\pi D$ of the phase moving across the aperture according to an approximate relationship $f_\phi \le f_c \le 3f_\phi$. This yields an estimate for the cutoff frequency in terms of the Greenwood frequency and D/r_0 via

$$f_\phi = 0.745 \frac{f_G}{D/r_0}.$$

In this work, we use a cutoff frequency $f_c = 6$ Hz corresponding to a Greenwood frequency of 30 Hz with $D/r_0 = 6$ and a roll-off of 30 dB/decade ($\alpha = 3$).[7].

The pdf describing the coupling efficiency depends on D/r_0 and the number of modes M guided by the fiber. The coupling efficiency for two fibers (10-mode and 69-mode) and turbulence conditions (D/r_0 = 2,4,6 and 9) was modeled using Monte Carlo simulations with Kolmogorov phase screens and simulated tilt compensation representing a fast-steering mirror (FSM).[7] [7] The fiber modes are modeled using LP modes for a step-index fiber (due to pairing of certain LP modes with the same cutoff frequency V_c, coupling into the 70-mode photonic lantern is modeled using a V-number producing a set of 69 scalar modes). The numerical results were then used to model the pdf based on a fit to an appropriate distribution. Generally, it was found that a Weibull distribution with two parameters,

$$w(x;\theta,k) = \frac{k}{\theta}\left(\frac{x}{\theta}\right)^{k-1} e^{-(x/\theta)^k}$$

was sufficient to fit the results in the various scenarios; however, as the efficiency becomes saturated the distribution transitions to a Gaussian narrowly peaked about the mean with negligible fading. The distributions obtained from best fit to the numerical results are listed in Table 1.

Table 1. PDF fitting with FSM in various conditions (* denotes distribution without FSM).

	$D/r_0 = 2$			$D/r_0 = 4$			$D/r_0 = 6$			$D/r_0 = 9$		
M	**PDF**	θ	k	**PDF**	θ	k	**PDF**	θ	k	**PDF**	θ	k
10	Weib.	0.76	32.1	Weib.	0.59	10.1	Weib.	0.41	5.17	Weib.	0.23	3.50
69	Gauss. (μ=0.89, σ=5E-3)			*Weib.	0.86	67.3	Weib.	0.80	44.6	Weib.	0.66	16.7

Table 2 summarizes the distributions in terms of the mean coupling efficiency and "peak" fade depth relative to the mean bounding 99.99% of the received power. The latter is calculated using the cumulative distribution function $W(x;\theta,k) = 1 - e^{-(x/\theta)^k}$. For system testing, two scenarios were emulated in hardware (D/r_0 = 4 and 9). Note that the peak fade depth for the 10-mode fiber is 3 – 9 dB larger than the 69-mode fiber in this range.

Table 2. Mean coupling efficiency (CE) and 99.99% fade depth (FD) of pdfs in Table 1.

$M\backslash(D/r_0)$	**2**		**4**		**6**		**9**	
	Mean CE	**99.99% FD**	**Mean CE**	**99.99% FD**	**Mean CE**	**99.99% FD**	**Mean CE**	**99.99% FD**
10	0.75	1.19 dB	0.56	3.75 dB	0.38	7.37 dB	0.2	11.0 dB
69	0.89	0.09 dB	0.85	0.56 dB	0.79	0.84 dB	0.64	2.26 dB

5. TEST SETUP

A block diagram of the test setup is shown in Figure 2. The test optical transmitter[3] generates the CCSDS HPE waveform and is used to emulate the signal sent from the spacecraft. The free-space path loss is emulated with two variable optical attenuators (VOAs) in series. A power meter is used to monitor the power into the receiver system. The fade emulation system described in section 3 is used to modulate the transmitted signal with emulated channel fades. The fade emulation system was connected directly to the FMF used in the array architecture. A free-space fiber coupler was used to send light into the photonic lantern. Note that the average fiber coupling loss induced by atmospheric turbulence is not emulated in the test setup. Table 3 shows independent measurements of the average additional losses expected for the tested conditions. The test setup for these measurements was documented by Vyhnalek and Tedder.[11]

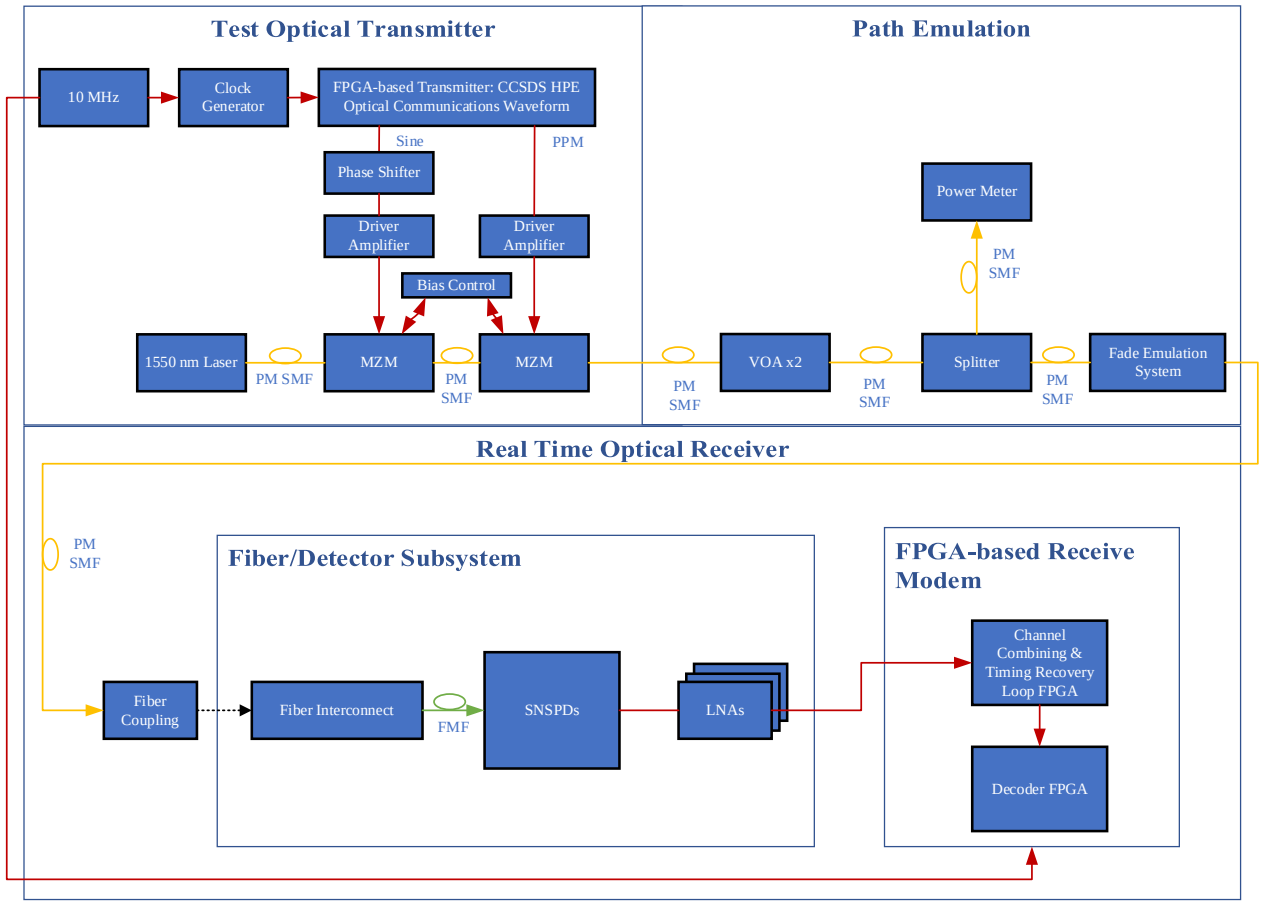

Figure 2. Block diagram of the real time optical receiver system within the optical communications test bed.

Table 3. Measured average additional fiber coupling induced loss.

Fiber Interconnect	$D/r_0 = 4$	$D/r_0 = 9$
10-mode fiber	4.8 dB	10.6 dB
70-mode photonic lantern	2.9 dB	5.5 dB

6. FADE EMULATION TESTING RESULTS

Two fading channel scenarios, shown in Table 4, were tested with each receiver architecture. Both scenarios have the same pointing and scintillation-induced fading but the coupling-induced fading was varied. Scenario 1 emulated a D/r_0 of 4 and scenario 2 emulated a D/r_0 of 9. The receiver mode tested was the PPM-32, code rate 1/3 mode. This mode was tested with three different slot widths: 2 ns, 1 ns, and 0.5 ns. These slot widths correspond to data rates of 21 Mbps, 42 Mbps, and 83 Mbps. Four different channel interleaver sizes were tested with each slot width. The interleaver has $N = 84$ rows and each row, i, is of length iB, where $B \in \{0, 540, 2160, 4140\}$. Results in Figures 3-5 contain the average results across all four interleaver sizes. The interleaver size does not impact the acquisition performance and should have no impact on the codeword error rate results in the presence of no emulated channel fades.

Table 4. Two fade scenarios ($D/r_0 \in \{4,9\}$) were tested with both receiver architectures. The power scintillation index, σ_I^2, HWHM atmospheric correlation time, τ_C, and pointing jitter distribution β, were kept constant.

Fade Scenario	**Power Scintillation Index, σ_I^2**	**Atmospheric Correlation Time, τ_c**	**Telescope Coherence Ratio, D/r_0**	**Pointing Jitter Distribution β**
1	0.025	1 ms	4	16
2	0.025	1 ms	9	16

6.1 Baseline performance without fading

The timing recovery loop baseline acquisition power levels and the power levels at which the codeword error rate is 10^{-4} without fading are shown in Figure 3 for both receiver architectures. The acquisition power level is defined as the minimum power level at the input to the fiber coupler at which the receiver timing recovery loop acquires and does not lose lock over a 1-minute measurement interval. The acquisition power level for the photonic lantern and 7 single pixel detector architecture is approximately 5 dB higher than for the FMF and detector array architecture in all three slot widths tested. The power required for a codeword error rate of 10^{-4} is approximately 4 dB higher for the photonic lantern and 7 single pixel detector architecture in all three modes tested. This performance difference in the two systems is attributed to the differences in the detectors used. There are less single pixel detectors used (7 vs. 15) and the single pixel detectors have a slower reset time than the detectors in the array.

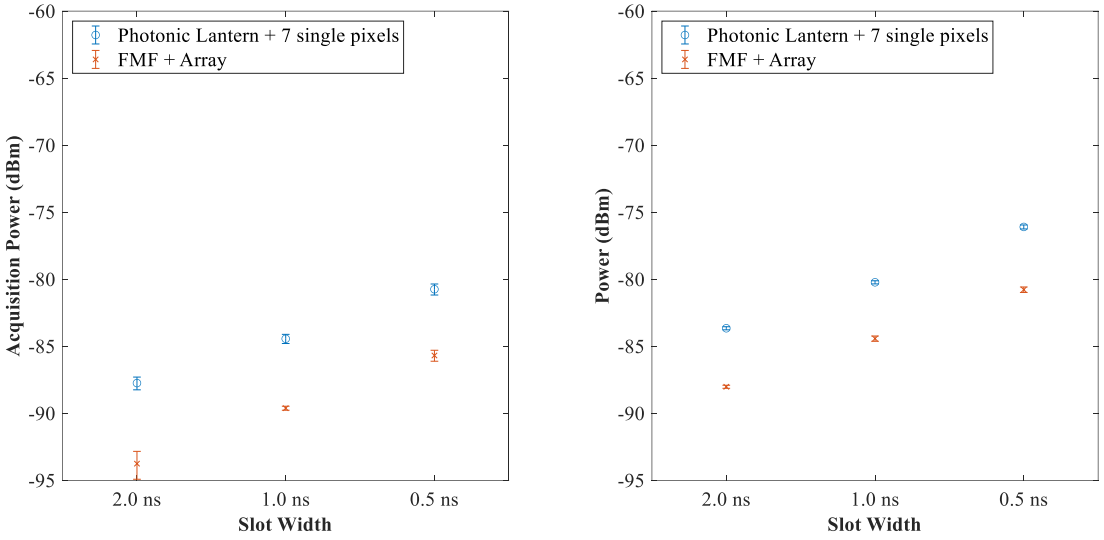

(a) (b)

Figure 3: Baseline performance without fading for PPM-32, code rate 1/3 mode with slot widths of 2.0, 1.0, and 0.5 ns. Figure (a) depicts the acquisition power threshold and figure (b) shows power level for a 10^{-4} CWER.

6.2 Acquisition performance with fading

The timing recovery loop acquisition loss due to fading is shown in Figure 4. The photonic lantern architecture requires 0-1 dB more power in both fading scenarios and across each slot width. However, the FMF and array architecture requires 2-3 dB more power in scenario 1 ($D/r_0 = 4$) and 9-12 dB more in scenario 2 ($D/r_0 = 9$).

The timing recovery loop acquisition performance in the presence of fading and fiber coupling loss is shown in Figure 5. The combined fading loss and fiber coupling loss is worse in both scenarios for the FMF and array architecture. When operating in the lower turbulence level of scenario 1 ($D/r_0 = 4$), the FMF and array architecture performs within 2 dB of

the photonic lantern architecture. Under scenario 2 ($D/r_0 = 9$) at higher turbulence conditions, the photonic lantern and 7 single pixel architecture performs 9-11 dB better than the FMF and array architecture.

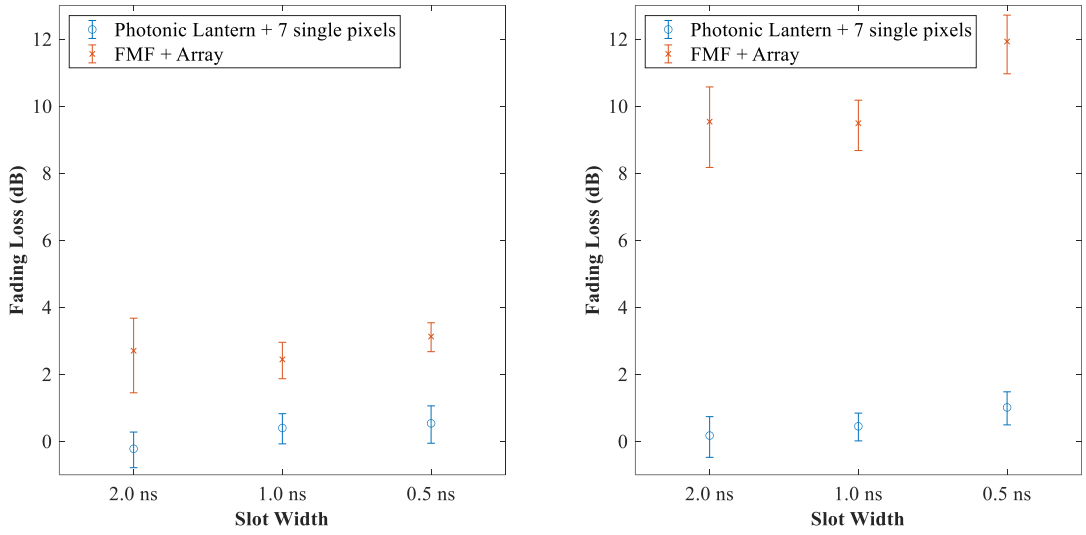

Figure 4. Additional power required due to fading above the baseline for the PPM-32, code rate 1/3 mode with slot widths of 2.0, 1.0, and 0.5 ns for fading (a) scenario 1 ($D/r_0 = 4$) and (b) scenario 2 ($D/r_0 = 9$).

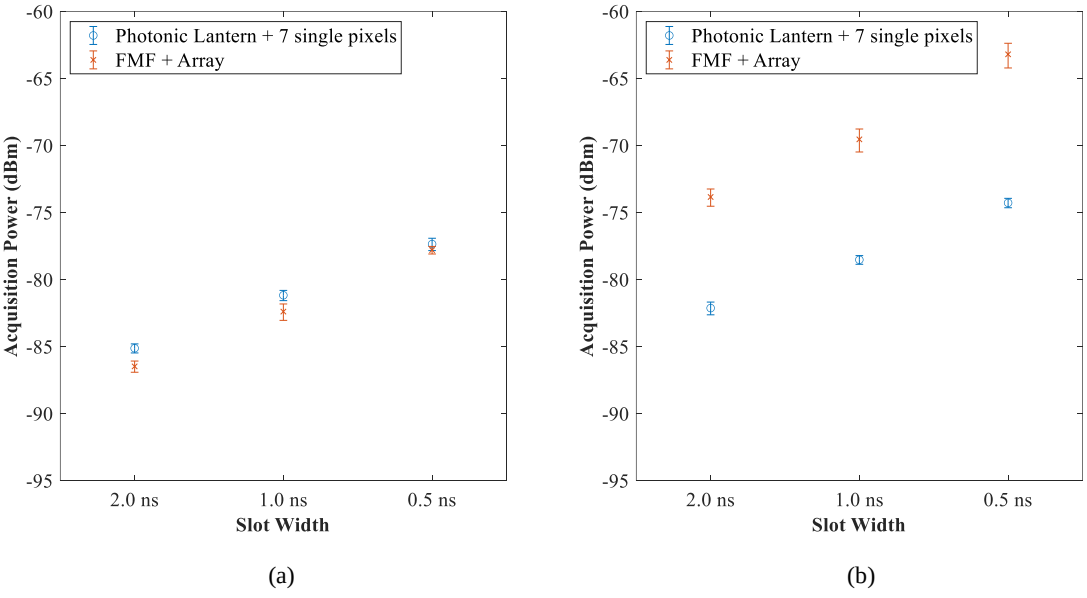

Figure 5. Required acquisition power in the presence of fading and fiber coupling loss for the PPM-32, code rate 1/3 mode with slot widths of 2.0, 1.0, and 0.5 ns in (a) scenario 1 ($D/r_0 = 4$) and (b) scenario 2 ($D/r_0 = 9$).

6.3 Codeword error rate and throughput performance

Codeword error rate curves with four different convolutional interleaver sizes ($B \in \{0, 540, 2160, 4140\}$) and both fading scenarios were measured. Each codeword error rate point was taken for at least one minute and contains a minimum of 100 codeword errors. The average signal photons per signal slot, K_s, from each minute is used to place the codeword error rate data collected each minute into K_s bins sized 0.025 dB apart.

The codeword throughput was also calculated across the receiver dynamic range. Step sizes of 1 dB were used to find the receiver dynamic range and step sizes of 0.2 dB were used over transition between 0% throughput to 100% throughput. Between steps, the receiver was held in reset and released 2.1 seconds after the transmitter started modulating the carrier so that the receiver would always have a valid signal at acquisition. The codeword throughput was calculated from the number of transmitted codewords and the number of received codewords over a 1 minute interval.

Figure 6 shows the normalized codeword throughput and the codeword error rate curves for fade scenario 1 ($D/r_0 = 4$) and both architectures in the PPM-32, code rate 1/3, 0.5 ns slot, 83 Mbps mode. The baseline throughput and codeword error rate curve without fading for $B = 4140$ is also shown. The codeword error rate curves show that as the interleaver size increases, the codeword error rate improves. This is also reflected directly in the codeword throughput curve. The photonic lantern and 7 single pixel architecture shows an improvement of approximately 1.5 dB between the curve taken without interleaving ($B = 0$) and the curve with the largest interleaver ($B = 4140$). The FMF and array architecture shows an improvement of almost 3 dB.

The codeword error rate and throughput curves for fade scenario 2 ($D/r_0 = 9$) is shown in Figure 7 for both architectures and the PPM-32, code rate 1/3, 0.5 ns, 83 Mbps mode. Results for the photonic lantern and seven single pixel detectors are similar to scenario 1 – the performance loss due to fading is approximately 0.5 dB with the largest interleaver. For the FMF and array architecture, the codeword error rate curve shows that with the largest interleaver size ($B = 4140$), there is a performance improvement to within 1.5 dB of the baseline curve. However, the throughput at this point is only ~90%. This is because the fades in this case are so deep that receiver loses acquisition and must reacquire. The time to reacquire with large interleaver sizes is significant and causes a loss of throughput. In fact, the throughput for the $B = 4140$ curve is worse than for the $B = 540$. Performance of the receiver in this case is driven by the timing recovery loop minimum acquisition power.

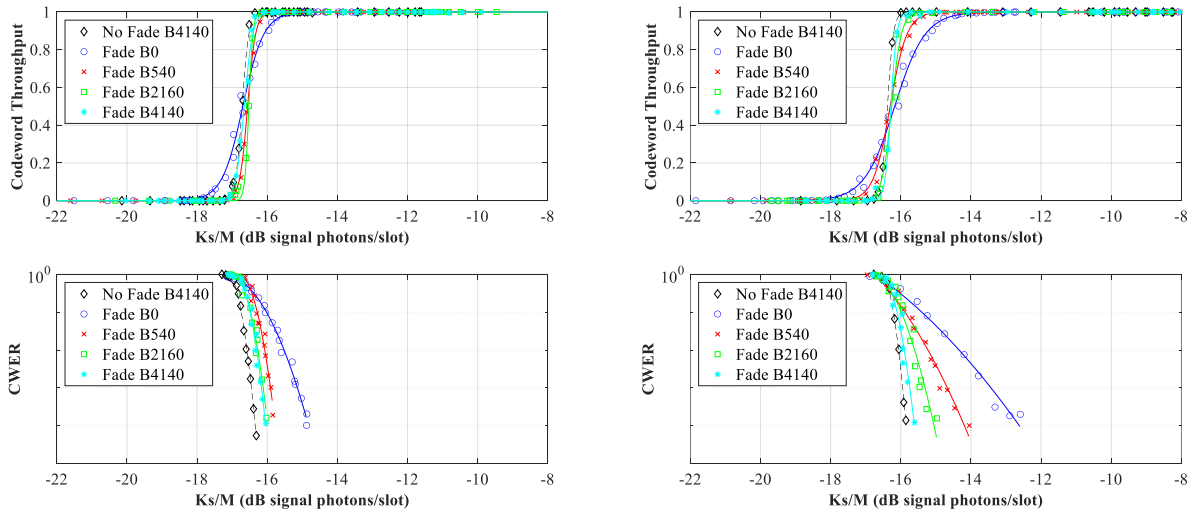

Figure 6. Scenario 1 (D/r_0=4) test results with (a) photonic lantern + 7 single pixel architecture and (b) FMF + array architecture

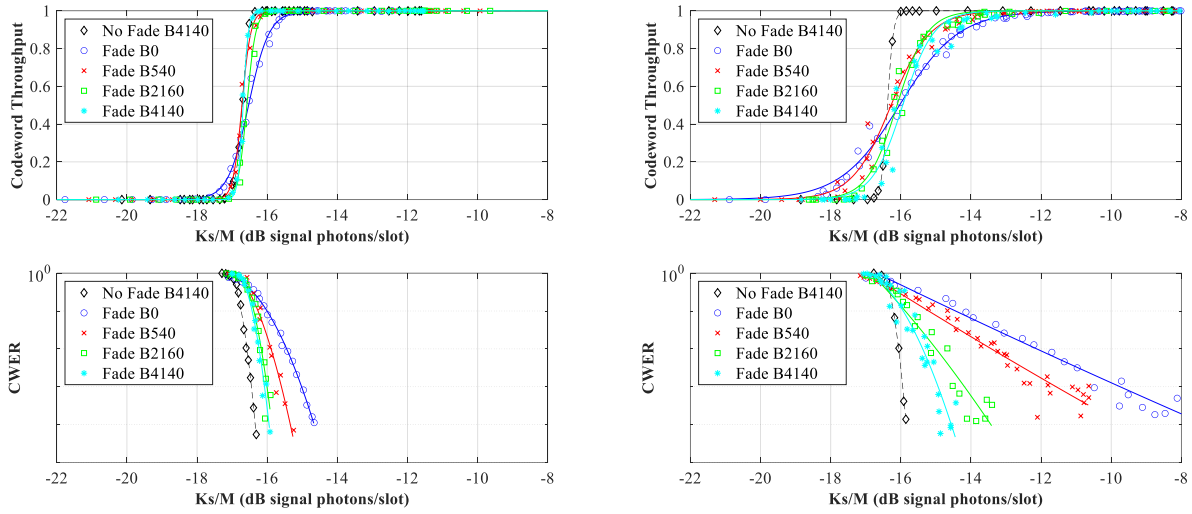

(a) (b)

Figure 7. Scenario 2 (D/r_0=9) test results with (a) photonic lantern + 7 single pixel architecture and (b) FMF + array architecture

6.4 Comparison of predicted results to hardware test results

When the receiver loses acquisition due to a fade, a complete flush of the interleaver occurs. This can take approximately 0.58 seconds to complete for the PPM-32, 0.5 ns slot width with the largest interleaver ($B = 4140$), so high receiver availability can only be maintained if fades below the acquisition threshold occur very rarely, regardless of fade length. In the hardware tests, each fixed mean power level was maintained for 1 minute while fading was applied, so the minimum fade rate that can be measured is 0.0167 fades/second (1 fade every minute). Analysis of the level-crossing statistics for the synthesized fade vectors was used to estimate the acquisition margin required for a fade rate of 0.0167 fades/second or less. Results for both scenarios are given in Table 5. In several cases, this analysis predicts a larger fade margin than was actually seen in the hardware test. For example, it is predicted that the 69-mode fiber (photonic lantern) would need a margin of 3.9 dB for scenario 1 and 4.3 dB for scenario 2. This is about 3-4 dB greater than the results seen in hardware. The 10-mode fiber also requires about 3 dB less than predicted for scenario 1 and for the 2 ns and 1 ns slots in scenario 2. This analysis combined with the hardware tests shows that the receiver can tolerate some fades (~3 dB) below the acquisition threshold.

Table 5. Predicted acquisition margin, defined as fade threshold at which the fade rate drops below 0.0167 fades per second.

Fade Scenario	**10-mode fiber (Multi-pixel array)**	**69-mode fiber (Photonic lantern)**
1 $D/r_0 = 4 \mid \sigma_I^2 = 0.025 \mid \beta = 16$	5.3 dB	3.9 dB
2 $D/r_0 = 9 \mid \sigma_I^2 = 0.025 \mid \beta = 16$	11.9 dB	4.3 dB

7. CONCLUSION

A fade emulation system was used to emulate scintillation-induced, pointing-induced, and fiber coupling-induced fades in real time. This system was used to test a ground photon-counting receiver system consisting of a fiber interconnect, SNSPDs, and an FPGA-based receiver modem. Two different receiver architectures were tested with the PPM-32, code rate 1/3, CCSDS HPE mode. When operating without fades, the FMF and array architecture is better by 4-5 dB than the photonic lantern and 7 single pixel detector architecture because the array has more detectors with faster reset times. The fiber coupling-induced fade significantly impacted the performance of the architecture with the 10-mode FMF and detector array. In addition to the average fiber coupling loss reported in Table 3, this architecture required 9-12 dB more power due to fading to maintain acquisition in higher turbulence ($D/r_0 = 9$) than without fades. The 70-mode photonic lantern and single pixel architecture required 0-1 dB more power with fading to maintain acquisition in the same turbulence conditions. The 70-mode photonic lantern outperforms the 10-mode FMF by 9-11 dB in higher turbulence ($D/r_0 = 9$). In lower turbulence conditions ($D/r_0 = 4$), the 10-mode FMF performed better by 1-2 dB. If the single pixel detectors were equivalent in performance to the array detectors, the photonic lantern and single pixel detectors would outperform the array architecture in both cases. Analysis of predicted fades as compared to hardware test results showed that the receiver can operate with fades approximately 3 dB below the acquisition threshold. In the future, a more robust acquisition algorithm will be investigated to improve the performance of the receiver in deeper fading conditions.

8. ACKNOWLEDGEMENTS

This work was funded by the NASA Space Communications and Navigation program.

REFERENCES

[1] "Optical communications coding and synchronization recommended standard," CCSDS 142.0-B-1 Blue Book (2019).
[2] Hemmati, H. "Near Earth Laser Communications," CRC Press, Boca Raton, Florida, 2009.
[3] Downey, J., Tedder, S., Vyhnalek, B., Lantz, N., Marsden, M., Simon, W., Bizon, T., and Zeleznikar, D. "A real-time optical ground receiver for photon starved environments," Proc. SPIE 12413, Free-Space Laser Communications XXXV, 124130P (2023).
[4] Vyhnalek, B., and Tedder, S. "Fiber-detector subsystem loss comparison for a ground-based photon-counting optical receiver," Proc. SPIE 12413, Free-Space Laser Communications XXXV, 124130U (2023).
[5] Simon, W., Downey, J., Lantz, N., Bizon, T., Marsden, M., Vyhnalek, B., and Zeleznikar, D. "Field-programmable gate array implementation of a single photon-counting receive modem," Proc. SPIE 12877, Free-Space Laser Communications XXXVI, 12877-58 (2024).
[6] Katz, E., Chahine, Y., Vyhnalek, B., Tedder, S., "Acousto-optic modulator for emulating atmospheric fade in free-space optical communication systems," Proc. SPIE 11272, Free-Space Laser Communications XXXII, 1127219 (2020).
[7] Chahine, Y., Katz, E., Vyhnalek, B., and Tedder, S., "Statistical analysis of fading power vectors for real-time atmospheric channel emulation," Proc. SPIE 12413, Free-Space Laser Communications XXXV, 124131L (2023).
[8] Epple, B., "Simplified channel model for simulation of free-space optical communications," J. Opt. Commun. Netw. 2, 293-304 (2010).
[9] Ellis, S., Bland-Hawthorn, J., and Leon-Saval, S., "General coupling efficiency for fiber-fed astronomical instruments," J. Opt. Soc. Am. B 38, A64-A74 (2021).
[10] Chahine, Y., Tedder, S., Staffa, J., and Vyhnalek B., "Optimal efficiency for passively coupling partially coherent light into mode-limited optical waveguides," J. Opt. Soc. Am. A 38, 1732-1743 (2021).
[11] Vyhnalek, B., Tedder, S., "Fiber-detector subsystem loss comparison for a ground-based photon-counting optical receiver," Proc. SPIE 12413, Free-Space Laser Communications XXXV, 124130U (2023).